RSC Advances

PAPER

View Article Online
View Journal | View Issue

Cite this: *RSC Adv.*, 2026, **16**, 23399

Bio-derived tannic acid-Eu(III) coordination synergizes with aluminum diethylphosphinate for low-loading and high-efficiency flame retardancy in PA66

Zongpin Liu,[abc] Wayne Hsu,[bc] Yincai Wu,[bc] Shenglong Wang,[bc] Junwei Zeng,[bc] Fenglong Lin *[bcd] and Lijun Song *[bcd]

A bio-derived europium–tannic acid complex (Eu@TA) was synthesized *via* a facile aqueous coordination strategy, leveraging the polyphenolic structure of tannic acid as a multidentate ligand and europium ions (Eu^{3+}) as the coordination center. This hybrid complex was melt-blended with aluminum diethylphosphinate (ADP) into a polyamide 66 (PA66) matrix to develop a synergistic low-loading flame-retardant system aimed at preserving the mechanical integrity of the pristine resin. With 8 wt% ADP and 2 wt% Eu@TA, the material reached a limiting oxygen index of 32.5% and achieved a UL-94 V-0 rating, and the peak heat release rate (PHRR) decreased to 318 kW m^{-2} with an increased fire performance index (FPI). Thermal analysis in air showed that the composite formed a stable carbonized layer at elevated temperatures, and the coordinated polyphenolic network favored a more compact char structure. Gas phase analysis further indicated that the system released fewer combustible volatiles during decomposition. The material retained about 97.6% of the tensile strength and about 87.8% of the impact strength of the neat sample, reflecting a largely preserved mechanical response. Because tannic acid has long been used in biological macromolecule modification and biointerfaces, the Eu@TA approach provides a bio-derived option that can be extended to polymer systems requiring both fire resistance and compatibility with biopolymer components.

Received 9th March 2026
Accepted 21st April 2026

DOI: 10.1039/d6ra02012g

rsc.li/rsc-advances

1. Introduction

Polyamide 66 (PA66) is widely used in automotive parts, electrical devices, mechanical assemblies, and industrial fibers due to its high strength, abrasion resistance, solvent tolerance, and heat-deflection stability.[1–4] Despite these advantages, its limiting oxygen index of ~21–24% makes it readily flammable, and the pronounced melt-dripping behavior during burning further escalates secondary ignition risks.[5] These issues limit its use in applications that require strict fire-safety standards, such as transportation interiors, aerospace components, and compact electrical housings.[1,6] To mitigate these hazards, numerous flame-retardant systems have been introduced. Halogenated additives were once effective but are now being phased out due to the corrosive and toxic byproducts formed during combustion. This shift has led to a strong demand for halogen-free systems.[7,8]

Among them, phosphorus-based flame retardants have drawn broad research interest. Aluminum diethylphosphinate (ADP) is one of the most studied phosphorus-based flame retardants because it functions in both gas and condensed phases.[9–11] During decomposition, ADP generates PO· and HPO· radicals that quench active gas-phase radicals, while the residual phosphorus species promote char formation, producing a barrier that slows heat transfer and restricts oxygen diffusion.[12] Previous studies have demonstrated that incorporating nanometric metal oxides with ADP triggers a strong synergistic effect, significantly enhancing the overall flame retardancy.[13,14] Similarly, Naik *et al.* reported that in glass-fiber-reinforced PA66, a total loading of only 15 wt% of ADP combined with melamine-integrated metal phosphates (2 : 1 ratio) achieves a UL-94 V-0 rating and significantly reduces the heat release rate.[15] A. R. Horrocks *et al.* reported that 15 wt% AlPi passes the UL-94 V-0 rating.[10] In a subsequent report, Zhan *et al.* achieved a UL-94 V-0 rating for PA66 using only 7 wt% ADP combined with 3 wt% sepiolite (a total loading of 10 wt%).[12]

Bio-based flame retardants have gained significant interest due to their renewability, lower toxicity, and compatibility with

[a]*School of Chemistry and Materials, Fujian Normal University, Fujian, 350007, China*
[b]*State Key Laboratory of Structural Chemistry, Fujian Institute of Research on the Structure of Matter, Chinese Academy of Sciences, Fuzhou, Fujian, 350002, China. E-mail: linfenglong@fjirsm.ac.cn; slj@fjirsm.ac.cn*
[c]*Xiamen Key Laboratory of Rare Earth Photoelectric Functional Materials, Xiamen Institute of Rare Earth Materials, Chinese Academy of Sciences, Xiamen, Fujian, 361021, China*
[d]*Fujian College, University of Chinese Academy of Sciences, Fuzhou, 350002, China*

biological macromolecule-related materials.[16] Tannic acid (TA), a plant-derived polyphenolic macromolecule, is widely used in protein, polysaccharide, and cellulosic surface modification and is frequently employed in biomedical coatings, protective barriers, and biointerfaces. Its catechol and galloyl groups enable strong intermolecular interactions and provide both carbon-forming and gas-expansion functions during thermal decomposition.[16,17] These features contribute to a compact char layer, which is valuable for polymer systems that require flame resistance while maintaining compatibility with bio-related components.

Rare-earth elements such as Eu^{3+} exhibit Lewis acidity and strong coordination capability. They can catalyze dehydration, crosslinking, and aromatization reactions during polymer pyrolysis, lowering the onset temperature for char formation and improving the structural robustness of the carbonized layer[7,18] When TA is coordinated with Eu^{3+}, the resulting complex simultaneously offers a polyphenolic carbon source and catalytic activity. This molecular arrangement supports early char formation and increases char graphitization, which may restrict heat feedback and mass transport during combustion.[17,19,20] Although both TA and rare-earth compounds have been explored independently, relatively few studies have combined them into a single hybrid structure that takes advantage of their complementary functions. The inherent biocompatibility of tannic acid, widely utilized in biointerfaces and macromolecule modifications, enables the Eu@TA hybrid to maintain excellent interfacial compatibility with biopolymer components, paving the way for applications in biomedical and ecofriendly polymer systems.

Most reported flame-retardant designs still rely on simple physical mixtures of multicomponent additives. A coordinated Eu@TA structure provides a different approach in which the organic and inorganic elements interact before blending into the polymer. Such a preassembled coordination network is expected to influence the thermal decomposition path of PA66 and may counterbalance the brittleness commonly induced by high phosphorus loadings. When further combined with ADP, a multicomponent system can be formed that distributes gas-phase radical trapping, condensed-phase catalytic charring, carbon-source supply, and inert-gas release across a unified mechanism. Leveraging the renewable and plant-derived nature of tannic acid, the Eu@TA complex represents a sustainable bio-derived flame retardant that minimizes environmental impact while enhancing the fire safety of polyamide 66 without compromising its recyclability.

This work presents an Eu@TA hybrid prepared *via* a simple aqueous coordination route and introduces it together with ADP into PA66. The study evaluates how this combination affects the ignition behavior, heat-release characteristics, char morphology, gas-phase evolution, and mechanical properties. This approach also provides a framework for constructing flame-retardant systems based on bio-derived polyphenols and rare-earth-assisted catalytic charring, which is relevant for polymer platforms that require fire resistance alongside compatibility with biological macromolecule-based materials.

2. Experimental

2.1 Materials

TA was supplied by Shanghai Huayuan Century Trading Co., Ltd. Europium(III) chloride hexahydrate ($EuCl_3 \cdot 6H_2O$) was obtained from Shanghai Titan Technology Co., Ltd. Polyamide 66 (PA66, grade EPR27) was bought from Pingdingshan Shenma Engineering Plastics Co., Ltd. ADP was provided by Wuhan Huaxiangkejie Biotechnology Co., Ltd. All reagents were used as received without further purification.

2.2 Synthesis of Eu@TA

Eu@TA was obtained through direct coordination in water. 1.7 g of tannic acid and 0.6 g of europium chloride were respectively dissolved in 200 mL and 50 mL of deionized water. The aqueous tannic acid solution was stirred using a magnetic stirrer, and the aqueous europium chloride solution was added dropwise under stirring. The mixture was stirred at 60 °C for 2 h to allow metal–polyphenol coordination. The resulting dispersion was cooled, centrifuged, and washed several times with water to remove unbound ions. The solid was dried at 60 °C to a constant weight. The micromorphology of the complex is shown in Fig. S1.

2.3 Preparation of composite materials

Before processing, the PA66, ADP, and Eu@TA powders were dried under a vacuum at 80 °C for 12 h. After drying, the components were premixed and compounded using a twin-screw extruder operated at 250–265 °C with a screw speed of 120 rpm. The extrudate was pelletized and dried again before molding. Standard test specimens were prepared by injection molding at 265 °C with a mold temperature of 80 °C. The sample codes reflect the additive content in weight percent, as shown in Table 1.

2.4 Characterizations

Fourier transform infrared (FTIR) spectroscopy was conducted in the ATR mode using an infrared spectrometer (Thermo Nicolet iS50 spectrometer). The scanning range was from 4000 to 525 cm^{-1}, and the spectral resolution was set to 4 cm^{-1}. The elemental content of Eu in the Eu@TA complex was analysed using an inductively coupled plasma emission spectrometer (ICP-OES, JY-Horiba ICP-OES Ultima 2). Additionally, C, H, and O contents were measured using an elemental analyser (EA, Elementar Vario EL Cube). X-ray photoelectron spectroscopy (XPS, Thermo Scientific K-Alpha) was used to test the elemental state and composition of the Eu@TA flame retardant using Al Ka excitation radiation ($h\nu$ = 1486.6 eV and 15 W). Thermogravimetric analysis (TGA) tests were performed using a Mettler-Toledo TGA instrument under both air and Ar conditions. Typically, samples weighing 3–5 mg were heated from room temperature to 800 °C at a heating rate of 10 °C min^{-1} during TGA.

The LOI test was conducted using a critical digital oxygen index analyser (TTech-GBT2406-4, TESSTECH (Suzhou) Testing Instrument Technology Co., Ltd). Samples measuring 125 mm × 6.5 mm × 3 mm were prepared and tested following the

Table 1 Results of the UL-94 and LOI tests for neat PA66 and the PA66 composites

	Composition (wt%)					UL-94			
Sample	PA66	ADP	Eu@TA	TA	LOI	t_1/t_2[a]	Dripping	Cotton	Rating
PA66	100	—	—	—	25.5 ± 0.2	>30	Yes	Yes	NR[b]
PA66-1	91	9	—	—	30.9 ± 0.1	>30	Yes	Yes	NR
PA66-2	90	10	—	—	31.7 ± 0.2	>30	Yes	Yes	NR
PA66-3	89	11	—	—	32.7 ± 0.1	>30	Yes	Yes	NR
PA66-4	86	14	—	—	34.8 ± 0.2	11.0/13.7	No	No	V-1
PA66-5	85	15	—	—	34.9 ± 0.3	3.7/4.2	No	No	V-0
PA66-6	91	7	2		31.3 ± 0.1	18.33/4.3	Yes	Yes	V-2
PA66-7	90	8	2	—	32.5 ± 0.1	6.0/4.0	No	No	V-0
PA66-8	89	9	2	—	34.7 ± 0.2	1.0/2.6	No	No	V-0
PA66-9	91	7	—	2	30.2 ± 0.3	>30	Yes	Yes	NR
PA66-10	90	8	—	2	31.1 ± 0.1	>30	Yes	Yes	NR

[a] t_1 and t_2 are the average combustion times after the first and second applications of the flame, respectively. [b] No rating.

procedures outlined in ISO 4589-2:2017. The vertical burning rating was assessed using a horizontal-vertical burning tester (TTech-GBT2408, TESSTECH (Suzhou) Testing Instrument Technology Co., Ltd). Samples measuring 125 mm × 13 mm × 3 mm were prepared and tested in accordance with the procedures outlined in ASTM D3801-2020a. The reaction-to-fire of the composite material was evaluated using a cone calorimeter (CCT, Mortis Combustion Technology (China) Co., Ltd). Samples measuring 100 mm × 100 mm × 3 mm were prepared and tested with a calibrated radiation power of 35 kW m^{-2} following the procedures outlined in ISO 5660-5:2016. The mechanical properties of the composite material were assessed using a universal material testing machine (Instron 2365 (5 kN)). Rectangular samples measuring 75 mm × 5 mm × 2 mm were prepared and subjected to tensile testing at a rate of 50 mm min^{-1} following the procedures outlined in ISO 527-2:2012. Notched impact tests of PA66 composites were conducted using an impact tester (SANSZBC1400-2). Rectangular specimens of a standard size were used according to ISO 180:2019.

SEM (Apreo S LoVac) with energy-dispersive spectrometry (EDS) was used to semiquantitatively analyze the components of the char residue of PA66 composites after cone calorimetric tests. A Raman spectrometer (BWS465-785S) excited by a 785 nm laser was used to measure Raman spectra to investigate the degree of graphitization of char after conical calorimetry tests. In order to analyze the pyrolysis product of the flame-retardant PA66 blends, TGA was coupled with Fourier transform infrared spectroscopy (TG-IR, Thermo Fisher Nicolet iS10 FTIR spectrometer, Germany), and the sample was heated from 30 °C to 800 °C in an N_2 flow. The spectra were obtained with a scan interval of 10 s, and the wavelength acquisition range of the infrared spectrum was from 500 to 4000 cm^{-1}.

3. Results and discussion

3.1 Characterization of Eu@TA

The structure and composition of Eu@TA were examined by FTIR spectroscopy, TGA, XPS, and elemental analysis, as shown in Fig. 1 and Table 2. The FTIR spectra of TA and Eu@TA are presented in Fig. 1(a). For TA, the band at 1606 cm^{-1} is assigned to the aromatic C=C stretching vibration, and the band at 1307 cm^{-1} is related to the C–O stretching of phenolic groups. After coordination with Eu^{3+}, both bands shift slightly and broaden, indicating a change in the electronic environment of the aromatic rings and oxygen atoms.[21] The broad absorption centered around 3500 cm^{-1} is attributed to O–H stretching. The intensity of this band decreases noticeably in Eu@TA compared with TA, which is consistent with the partial deprotonation of phenolic hydroxyls and the formation of Eu–O bonds. These spectral changes support the formation of an Eu–polyphenol coordination network rather than a simple physical mixture.

The thermal stability of TA and Eu@TA in air is shown in Fig. 1(b). TA exhibits a rapid mass loss once heated above 200 °C and leaves only a small residue at 800 °C. For Eu@TA, the first mass loss stage occurs from room temperature to about 250–275 °C and is mainly attributed to the removal of physically adsorbed water and loosely bound volatile species. The total mass loss in this region is about 14%, which agrees with the presence of hydration water and residual solvents suggested by the elemental analysis.[22] In the second stage, the coordinated TA backbone starts to decompose, and thermally labile groups such as phenolic hydroxyl and ester linkages are cleaved. When the temperature approaches 400 °C, Eu^{3+} acts as a Lewis acid center and catalyzes the dehydration, crosslinking, and aromatization reactions of the TA ligand.[21,23] As a result, carbonization is promoted, and a stable carbonaceous residue forms. The final char yield of Eu@TA at 800 °C is much higher than that of TA, confirming that the introduction of Eu significantly improves the condensed-phase stability of the polyphenolic framework and provides an additional inorganic skeleton for the char.

XPS measurements further verify the coordination between Eu^{3+} and TA (Fig. 1(c and d)). The survey spectra show that Eu@TA contains C, O, and Eu on the surface, whereas TA contains only C and O. The O 1s signal of TA appears as a single broad peak centered near 531–532 eV, which reflects the overlap of phenolic –OH and C–O contributions. After coordination, the O 1s peak of Eu@TA becomes broader and slightly shifts, indicating the presence of multiple oxygen environments. The deconvolution of the Eu@TA O 1s region reveals contributions

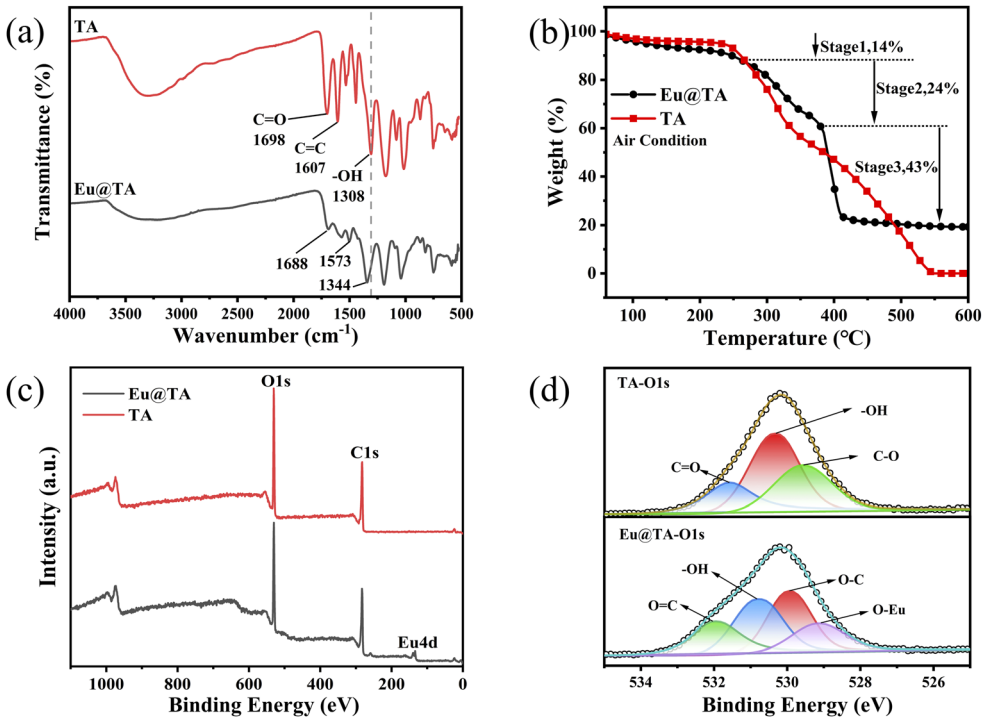

Fig. 1 (a) FTIR spectra of TA and Eu@TA. (b) TG curves of flame-retardant agents under air conditions. (c) XPS spectra of TA and Eu@TA. (d) High-resolution O 1s spectra of TA and Eu@TA.

Table 2 Elemental composition of the Eu@TA complex

		Contents (wt%)	
Method	Element	Theoretical	Experimental
EA	C	39.255	38.930
	O	44.034	43.346
	H	3.641	3.648
ICP-OES	Eu	13.070	12.790
Total	—	100.00	98.714

from Eu–O, C–O, and C=O species.[24,25] The Eu 3d region (not shown here in detail) displays characteristic Eu $3d_{5/2}$ and Eu $3d_{3/2}$ peaks, confirming that europium is present in an oxidized state and participates in coordination with the polyphenolic ligand. All binding energies fall in the expected ranges for organic oxygen and Eu–O bonds, which supports the proposed structure of Eu@TA.

Elemental analysis data are summarized in Table 2. The experimental carbon, hydrogen, and oxygen contents obtained by EA are close to the calculated values for the designed Eu–tannic acid complex. The Eu content measured by ICP-OES is also in good agreement with the theoretical value. The total mass fraction approaches 100%, and the small deviation can be ascribed to residual moisture and experimental uncertainty. Taken together with the FTIR, TGA, and XPS results, these data indicate that Eu@TA is a well-defined Eu–polyphenol coordination complex with higher thermal stability and a higher char-forming tendency than the original tannic acid, which is favorable for its use as a condensed-phase active component in flame-retardant systems.

3.2 Flame retardancy of Eu@TA

The flame retardancy of PA66 and its composites was evaluated by LOI and UL-94 vertical burning tests, and the results are summarized in Table 1. Neat PA66 burns readily once ignited, with an LOI of 25.5%, severe melt-dripping, and little solid residue. The molten material easily ignites the adjacent cotton, indicating poor inherent flame resistance.

When ADP is added alone, the flame retardancy improves, but it requires a relatively high loading to suppress melt-dripping. At 14 wt% ADP, dripping is minimized, and at 15 wt% ADP, the sample reaches a V-0 rating. These results show that ADP is effective but usually demands a large dosage to compensate for the lack of structural integrity in PA66 during burning.

The introduction of Eu@TA allows for a substantial reduction in the ADP content while maintaining a high flame-retardant level. With 8 wt% ADP and 2 wt% Eu@TA, the LOI increases to 32.5%, and the composite reaches a V-0 rating without melt-dripping. The increased LOI can be attributed primarily to the catalytic effect of Eu@TA, which promotes early crosslinking and charring during polymer pyrolysis, leading to the formation of a more coherent condensed-phase barrier that restricts the release of flammable volatiles.[26,27] Although the PA66-8 sample (containing 9 wt% ADP) shows a slightly higher LOI and a shorter after-flame time, PA66-7 successfully achieves a V-0 rating and completely suppresses melt-dripping with an even lower ADP loading of 8 wt%. The fact that melt-dripping is eliminated at such a low ADP content – especially when compared to the severe dripping observed in samples with higher ADP-only loadings – demonstrates that Eu@TA does not

act solely through gas-phase radical effects but also profoundly influences the physical behavior of the polymer in the condensed phase during combustion. Eu@TA exhibits synergistic interactions with the decomposition products of ADP. Specifically, the Eu species react with the phosphinic acid derivatives generated from ADP, acting as cross-linking agents that catalyze the charring of the PA66 matrix. This process facilitates the formation of a robust and continuous carbonized layer, which serves as a superior physical barrier to inhibit the release of flammable volatiles and protect the underlying polymer during pyrolysis.[28,29] In addition, the distribution of Eu in the cross-section of PA66-7, as shown in Fig. S8, is more uniform than that of the characteristic elements, P and Al, of ADP, which is one of the reasons for the better flame-retardant performance of PA66-7.

To further examine these effects, cone calorimetry was conducted (Fig. 2 and Table 3).[30] Neat PA66 shows a peak heat release rate (PHRR) of 670.6 kW m^{-2} and a total heat release (THR) of 94.9 MJ m^{-2}. For PA66-7, the PHRR decreases to 318.1 kW m^{-2}, and the THR decreases to 75.4 MJ m^{-2}. This corresponds to a 52.6% reduction in the PHRR and a 20.6% reduction in the THR relative to neat PA66. The delayed time-to-PHRR (*t*-PHRR), which increases from 264 s for neat PA66 to 333 s for PA66-7, indicates that the composite resists rapid flame spread and heat build-up more effectively than the untreated polymer.

Smoke production increases when ADP is introduced, which is typical for phosphorus-containing flame-retardant systems. With the same total flame-retardant content, PA66-7 exhibits a significantly higher smoke production rate than PA66-2 while remaining comparable to PA66-5. The Eu@TA-enhanced charring process, coupled with increased aromatization, results in the incomplete carbonization of the polymer matrix, which accounts for the elevated smoke production in PA66-7.

Table 3 Cone calorimetry test data of PA66 and its composites

Sample	PA66	PA66-2	PA66-5	PA66-7
PHRR (kW m^{-2})	670.6	499.7	376.7	318.1
THR (MJ m^{-2})	94.9	79.1	75.1	75.4
TTI (s)	108	124	107	105
t-PHRR (s)	264	322	302	333
FPI	0.161	0.248	0.284	0.330
TSP (m^2)	7.7	22.9	24.9	24.8
PSPR (m^2 s^{-1})	0.062	0.203	0.158	0.133
av-EHC (MJ kg^{-1})	26.11	21.78	20.67	21.01
RC (wt%)	1.35	6.93	13.68	11.55

The fire performance index (FPI), defined as TTI/PHRR, reflects the material's resistance to ignition hazards.[31] Neat PA66 shows an FPI of 0.161, while PA66-7's FPI increases to 0.330. This improvement correlates with the lower heat release rate and the more stable condensed-phase response. The enhanced FPI indicates that the Eu@TA/ADP system modifies both the ignition behavior and subsequent burning intensity.

Char residue analysis from cone calorimetry further clarifies the condensed-phase performance of the synergistic system. PA66-7 shows an increased char yield relative to neat PA66 and PA66-2, consistent with the TGA findings obtained under an argon atmosphere. This improvement verifies that Eu@TA interacts with both ADP degradation products and the polymer matrix to catalyze the formation of a sturdy cross-linked char layer during anaerobic pyrolysis. Additionally, a slight reduction

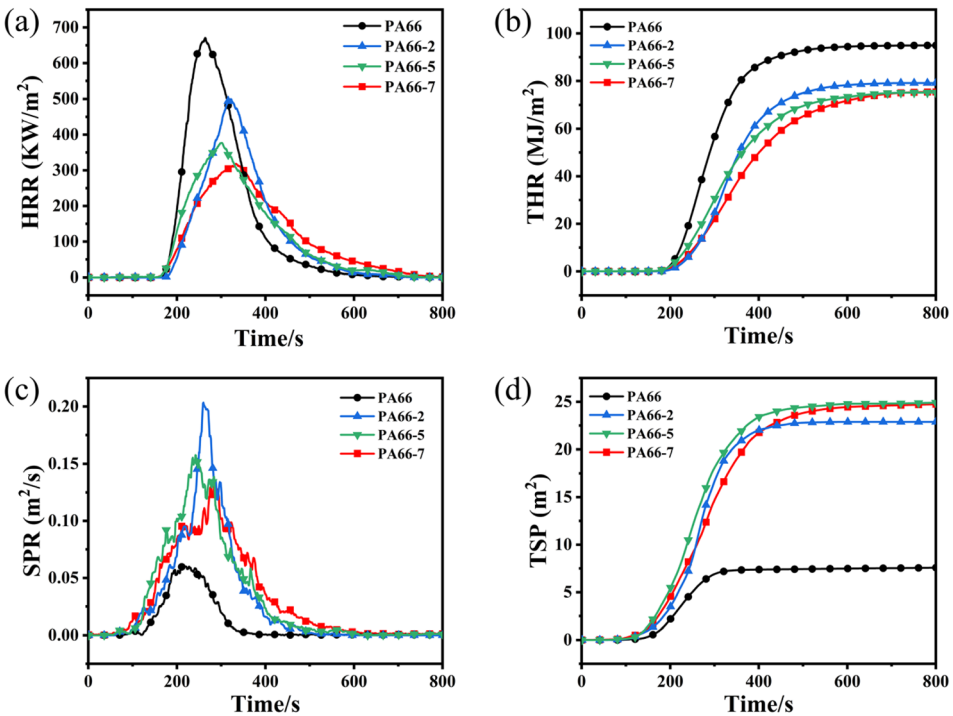

Fig. 2 (a) HRR *versus* time plots, (b) THR *versus* time plots, (c) SPR *versus* time plots, and (d) TSP *versus* time plots for PA66 and its composites.

in the average effective heat of combustion (av-EHC) is observed for modified samples compared to PA66-2. This indicates that the Eu@TA/ADP system functions by limiting the mass transfer of volatiles through the condensed phase while simultaneously diluting flammable species with inert gases and capturing gas-phase radicals. These combined effects diminish the total fuel supply, thereby lowering the PHRR.

3.3 Thermal stability of composites

The thermal decomposition behaviors of PA66 and its composites in an argon atmosphere were characterized by TGA and DTG (see the SI for the analysis and data under an air atmosphere), as illustrated in Fig. 3. The temperatures corresponding to the 5% mass loss and maximum mass loss rates are defined as $T_{5\%}$ and T_{max}, respectively.[32] The thermal decomposition of PA66 under an inert atmosphere is a complex process involving molecular chain scission, radical release, and subsequent char formation.[33]

The TGA and DTG curves of PA66 and its composites are presented in Fig. 3. As shown in the TG curves (Fig. 3(a)), neat PA66 exhibits obvious weight loss commencing at approximately 350 °C, undergoes intense decomposition within the 400–500 °C range, and yields a final char residue of less than 1%. Upon the incorporation of ADP, the char residue increases moderately; specifically, the char residue of PA66-5 reaches 1.55 wt% with increasing ADP loading, attributable to the catalytic carbonization effect of ADP on the polymer matrix.[12] Notably, with the further introduction of Eu@TA, the char residue of PA66-7 increases to 2.59 wt%, representing a significant enhancement compared to PA66-2, which contains the same total flame retardant loading. This improvement stems from the polyphenolic components providing additional carbon precursors, while Eu species facilitate the dehydration and cross-linking of polyamide fragments, ultimately remaining in the residual char as oxides.[34,35]

As observed from Table 4 and Fig. 3(b), the incorporation of flame retardants results in a gradual decrease in both $T_{5\%}$ and T_{max} of the composites. Compared to neat PA66, the $T_{5\%}$ values of PA66-2 and PA66-5 decrease by 20 °C and 26 °C, respectively. This phenomenon may be attributed to the catalytic effects of ADP and Eu@TA on the matrix at elevated temperatures, which promote decomposition pathways analogous to those of the base polymer, thereby inducing the premature thermal degradation of PA66. Additionally, PA66-7 exhibits a T_{max} of 401 °C, the lowest among all samples, indicating the effective suppression of the maximum mass loss rate.

In summary, the introduction of Eu@TA significantly modulates the thermal degradation behavior of the PA66/ADP/Eu@TA system by reducing the initial temperature of char formation and attenuating the maximum rate of thermal degradation.

3.4 Flame retardancy mechanism

The morphologies and structural characteristics of the char residues after cone calorimetry provide important evidence for understanding how Eu@TA influences the condensed-phase behavior of the composite. Fig. S3 and 4 display the macroscopic photographs and microscopic SEM micrographs of the char residues of the composites after cone calorimetry, respectively.

As depicted in Fig. S3, neat PA66 leaves virtually no residue following the cone calorimeter test, reflecting its poor inherent char-forming ability and the consequent failure to exert effective flame retardancy in the condensed phase. The incorporation of ADP improves the char yield of PA66-2; nevertheless, the resulting chars appear as fragmented pieces with poor integrity. With a higher ADP loading, PA66-5 displays enhanced char

Table 4 Typical thermal decomposition parameters of different samples under an Ar atmosphere

Sample	PA66	PA66-2	PA66-5	PA66-7
$T_{5\%}$ (°C)	388	368	362	360
T_{max} (°C)	430	411	409	401
V_{max} (%/°C)	1.62	1.38	1.51	1.19
RC (wt%)	0.95	1.13	1.55	2.59

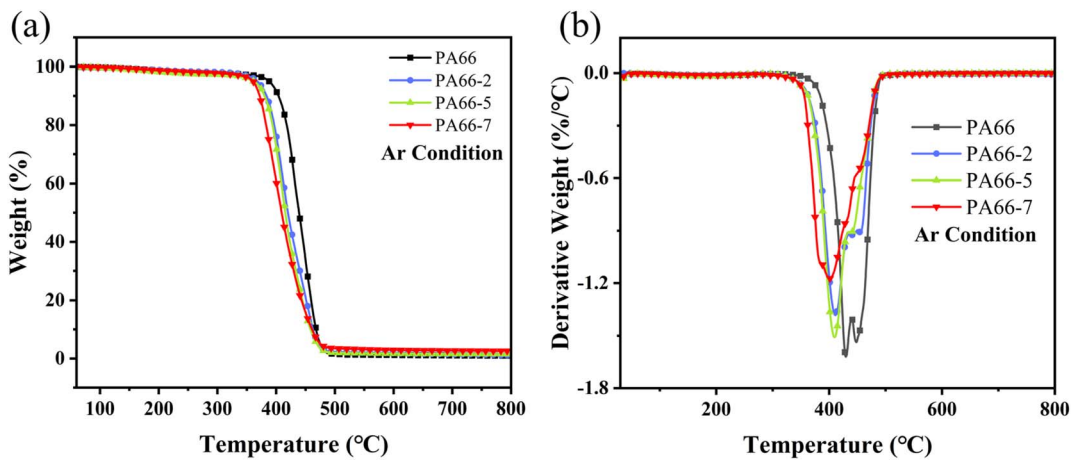

Fig. 3 (a) TG and (b) DTG curves of PA66 and the PA66 composites under an Ar atmosphere.

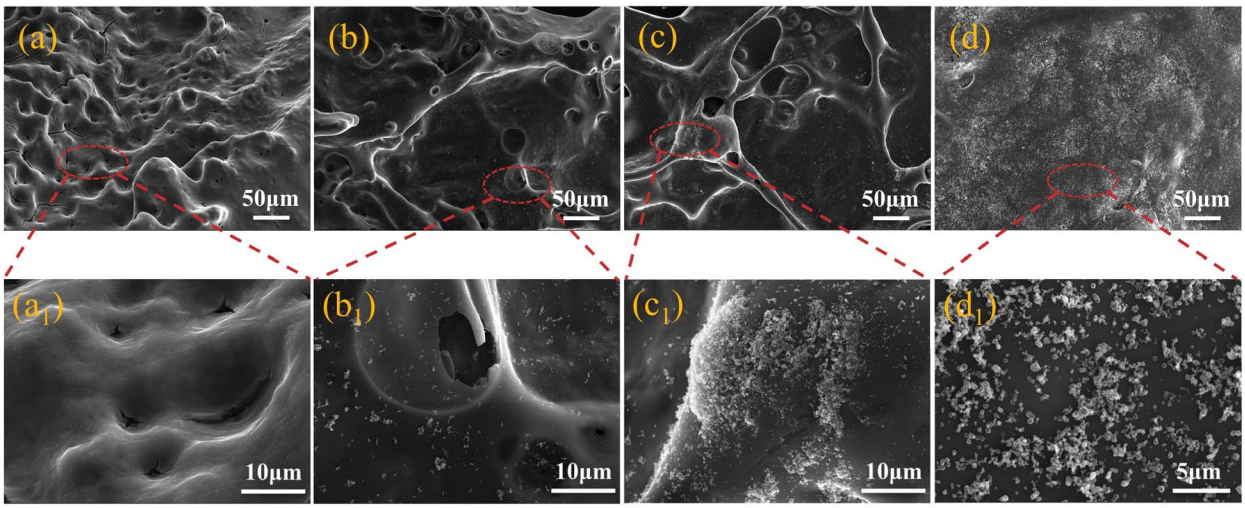

Fig. 4 SEM images of the outer surface of residual chars for PA66 (a and a_1), PA66-2 (b and b_1), PA66-5 (c and c_1) PA66-7 (d and d_1).

integrity and an increased char yield relative to PA66-2, partially explaining its superior flame-retardant rating. Notably, while the absolute char yield of PA66-7 is inferior to that of PA66-5, its macroscopic residue exhibits a more continuous and compact structure, serving as an effective physical barrier to restrict the transfer of heat and mass.

The SEM images of the residues are shown in Fig. 4. Neat PA66 leaves almost no coherent char, and the residue that remains consists of a fragmented, porous material with little structural integrity. Such a poorly connected char is ineffective in hindering the release of volatile fuels and heat transfer during burning.[7,36]

When ADP is introduced, the deposited char becomes somewhat more continuous, even though noticeable voids and ruptured regions are still present. As shown in Fig. 4(b and b_1), the char surface of PA66-2 is smoother than that of neat PA66, but its texture remains brittle and still exhibits obvious pores and fragmentation. With increasing ADP content, the surface pores and char fragmentation in PA66-5 are further reduced, but the char layer still lacks integrity. Additionally, Fig. $4c_1$ and S2 reveal that the phosphorus-rich char of PA66-5 is unevenly distributed. In contrast, as shown in Fig. 4(d and d_1), PA66-7 forms a dense and uniform layer with only minor surface defects. The char surface is flatter and shows fewer open pores, indicating that the composite develops a more stable carbonized structure as combustion progresses. This improvement is attributed to the catalytic effect of Eu species, which promotes dehydration and crosslinking reactions in the TA ligand and in the PA66 matrix as the temperature increases.[37]

The XPS analysis of the PA66-7 char (Fig. 5) provides further insights into the chemical composition of the residue. The signals in the C 1s spectrum corresponding to C–C/C–H, C–O/C–N, and carbonyl species indicate the partial thermal decomposition and cross-linking of the PA66 backbone.[38–40] The O 1s region includes components associated with C═O and C–O–P linkages, and the latter indicates the incorporation of phosphorus-containing species into the condensed-phase structure.[38] The presence of PO_x fragments in the P 2p spectrum confirms that ADP decomposes to generate polyphosphate-like species (Fig. S5), which are known to promote dehydration and carbonization. Furthermore, the Eu 3d spectrum reveals that Eu ultimately remains in the char residue in the stable +3 oxidation state (in the form of Eu_2O_3), which enhances the condensed-phase flame retardancy of the substrate to a certain extent. Based on the above analysis and Fig. S4, it can be inferred that in the presence of Eu species, these phosphorus-rich structures form a more tightly bound network, and inorganic Eu–O fragments can serve as additional crosslinking points within the char.

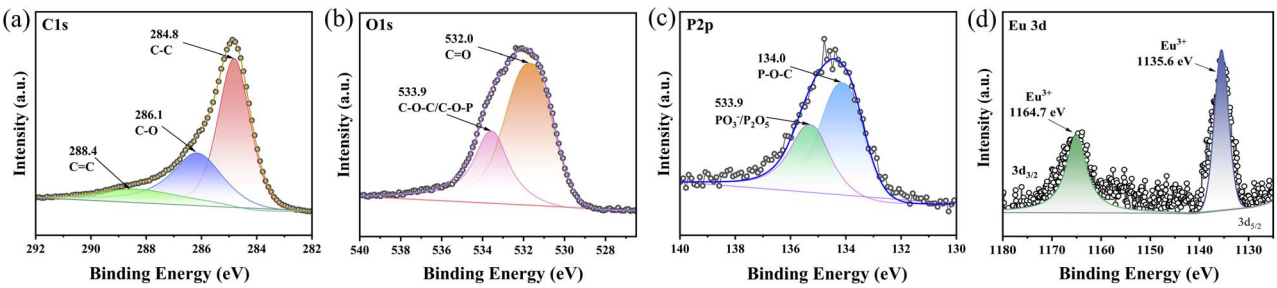

Fig. 5 XPS spectra of PA66-7 after the cone calorimeter test: (a) C 1s, (b) O 1s, (c) P 2p and (d) Eu 3d peaks.

The increase in char compactness is further supported by Raman spectra. Fig. 6 shows that all samples exhibit the characteristic D and G bands associated with disordered and graphitic carbon, respectively. For PA66, the I_D/I_G ratio is relatively high, indicating a predominantly disordered carbon residue.[41] The ratio decreases in PA66-5, and a further reduction is observed in PA66-7, reflecting a higher degree of structural ordering. This shift suggests that Eu-containing fragments participate in the rearrangement of decomposed polymer chains, favoring the formation of more extended conjugated structures.

The combined SEM, Raman, and XPS results show that Eu@TA contributes to char formation through two modes of action. First, the polyphenolic structure provides a carbon-rich source that readily undergoes condensation at elevated temperatures.[37] Second, the europium component catalyzes the structural evolution of both the TA-derived carbon and the decomposing PA66 chains, leading to increased rigidity and a higher degree of order in the final residue. These effects yield a continuous char layer with reduced porosity and improved mechanical stability, allowing it to remain intact during combustion and effectively resist melt-dripping. This behavior is consistent with the flame retardancy trends observed in the cone calorimetry tests, where PA66-7 exhibits markedly lower heat release rates and improved overall burning resistance.

TG-IR is commonly used to analyze gaseous products generated during thermal degradation, providing deeper insights into flame retardant mechanisms.[42] In this study, TG-IR spectroscopy was used to analyze the gas-phase composition of PA66 composites during pyrolysis. Fig. 7(a–c) presents the 3D TG-IR spectra of the gaseous pyrolysis products for pure PA66, PA66-5, and PA66-7 under a nitrogen atmosphere, respectively. Fig. 7(d–f) displays the FTIR spectra of the corresponding products at different degradation temperatures. Additionally, the TG and DTG curves obtained under a nitrogen atmosphere are shown in Fig. S6. The characteristic absorption peaks common to all three samples are as follows:

For pure PA66, the weak absorption peaks of CO_2 (668 cm^{-1} and 2356 cm^{-1}) are detected in the temperature range of 410–550 °C. Additionally, the absorption peaks corresponding to hydrocarbons (2738 cm^{-1}), ammonia (950 cm^{-1}), and carbonyl compounds (1766 cm^{-1}) are observed.[43] Upon the incorporation of ADP, alongside peaks similar to those of pure PA66, a distinct characteristic absorption peak of phosphorus oxides (1181 cm^{-1}) is observed within the 350–500 °C range. This indicates that the decomposition of ADP releases phosphorus oxides, which subsequently generate phosphorus-containing radicals. These radicals can effectively quench reactive oxygen and hydroxyl radicals ($O^{\bullet}$ and $OH^{\bullet}$), thereby terminating the combustion chain reactions.[44] Notably, PA66-7 exhibits absorption peaks similar to those of PA6-5 within the 400–510 °C range, which is consistent with the similar av-EHC values observed for PA66-5 and PA66-7 in the cone calorimetry tests.

As shown in Fig. S6, the gaseous products of PA66 and its composites at their maximum degradation temperatures (T_{max1} and T_{max2}) were analyzed by FTIR spectroscopy. For PA66-7, the absorption peak of NH_3 is observed at 950 cm^{-1}, indicating the release of inert nitrogen-containing compounds catalyzed by Eu@TA, which dilutes the concentration of small-molecule fuels. Furthermore, the characteristic P═O absorption peaks

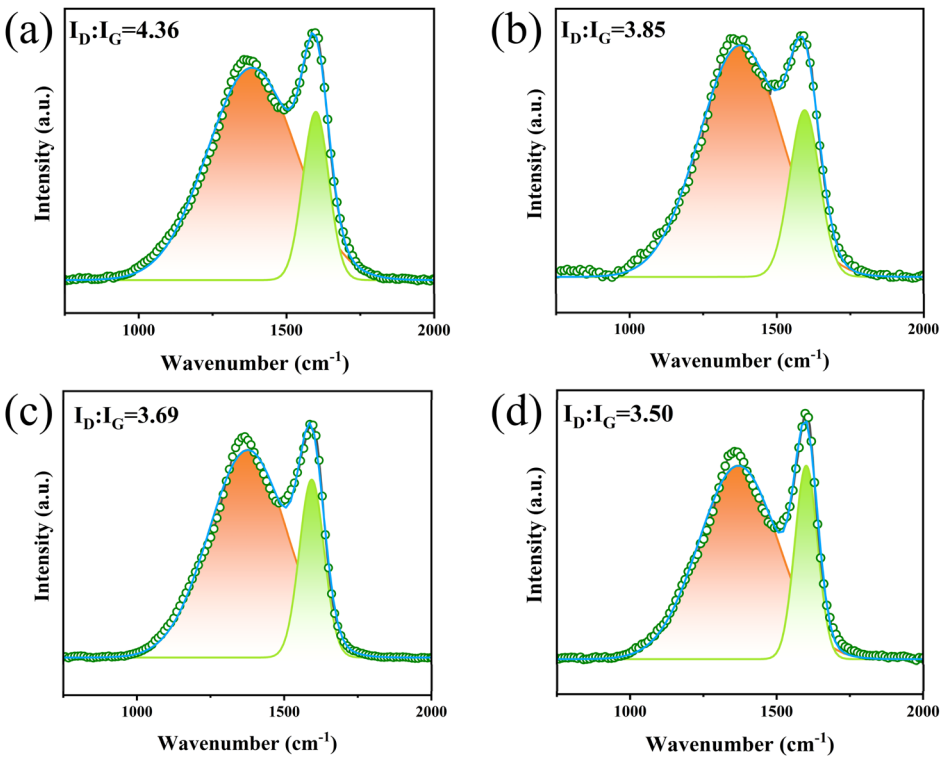

Fig. 6 Raman spectra of the PA66 composites: (a) PA66, (b) PA66-2, (c) PA66-5 and (d) PA66-7.

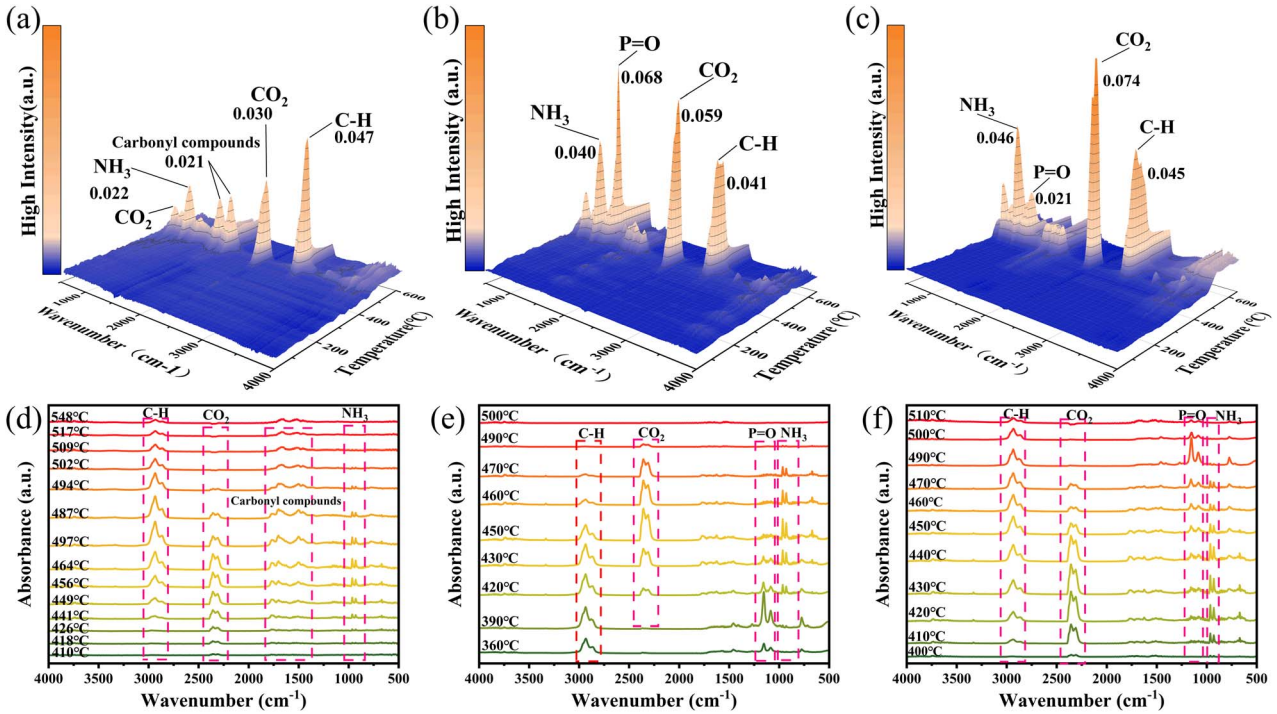

Fig. 7 3D images of the TG-IR results of (a) PA66, (b) PA66-5 and (c) PA66-7. IR spectra of the gaseous products of (d) PA66, (e) PA66-5 and (f) PA66-7 at various temperatures.

are detected in the decomposition products of both PA66-5 and PA66-7, resulting from the release of PO· and HPO· radicals during ADP decomposition. These radicals capture highly reactive H˙ and OH˙ species in the gas phase, thereby suppressing combustion.[9] Additionally, as shown in Fig. S6, the thermal decomposition characteristics of PA66, PA66-5, and PA66-7 in the TG-IR tests are similar to their thermal degradation behaviors in an argon atmosphere. The introduction of flame retardants, to some extent, influences the decomposition pathways of the matrix.

Thus, in the gas phase, PA66-7 effectively reduces the volume fraction of flammable components by releasing CO_2 and chemically stable nitrogen-containing compounds. Concurrently, structures such as P═O and P–O generate PO· and PO^{2-} radicals, which effectively quench reactive oxygen- and hydroxyl-containing radicals (O˙ and OH˙), thereby terminating the combustion chain reaction.[45]

3.5 Mechanical properties of the composites

As an excellent engineering plastic, PA66 is valued for its combination of high strength, high stiffness, and good thermal resistance. The mechanical properties of PA66 and its composites were evaluated through tensile and impact tests, as shown in Fig. 8 and Table 5. As illustrated in Fig. 8(a), the impact strength retention rate of PA66-7 reached 87.82%

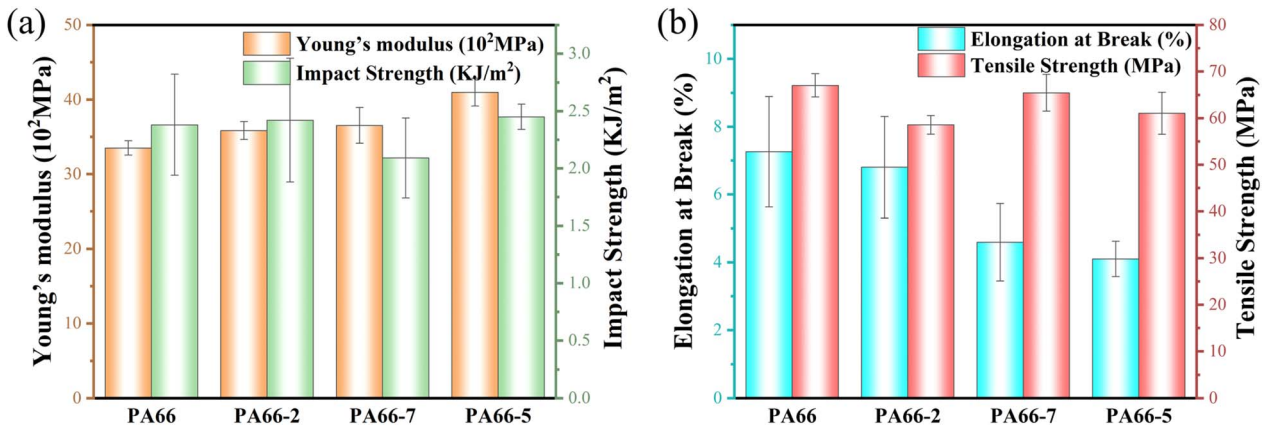

Fig. 8 (a) Impact strength and Young's modulus and (b) elongation at break and tensile strength of PA66 and its composites.

Table 5 Mechanical properties of the PA66 composites

Sample	PA66	PA66-2	PA66-5	PA66-7
Young's modulus (MPa)	3350.41 ± 96.93	3582.70 ± 120.26	4098.83 ± 184.5	3653.42 ± 239.06
Impact strength (kJ m^{-2})	2.38 ± 0.44	2.42 ± 0.54	2.45 ± 0.11	2.09 ± 0.35
Elongation at break (%)	7.26 ± 1.63	6.80 ± 1.50	4.10 ± 0.52	4.59 ± 1.14
Tensile strength (MPa)	67.04 ± 2.46	58.57 ± 2.01	61.07 ± 4.52	65.44 ± 3.93

compared to neat PA66, while the elastic modulus increased by 9.04%. These results indicated that the incorporation of ADP and Eu@TA had a negligible influence on the rigidity of PA66, allowing it to maintain the high strength and stiffness required for practical applications. As shown in Fig. 8(b), the tensile strength retention rate of PA66-7 was 97.61% relative to neat PA66. It was observed that the elongation at break of PA66 was affected by the addition of ADP. However, compared to PA66-5, PA66-7 achieved the same flame retardancy rating with a smaller reduction in both tensile strength and elongation at break. Furthermore, compared to the sample with 10% ADP, Eu@TA did introduce rigid complex particles, but at the cost of a slight reduction in toughness, it elevated the flame retardancy rating from No Rating (NR) to V-0. This trade-off is of great significance for practical applications.

4. Conclusions

A coordination-based hybrid flame retardant has been developed by reacting Eu^{3+} with tannic acid, and the resulting Eu@TA displays distinct thermal and structural features that differ from those of the parent components. When incorporated with ADP into PA66, the hybrid produces a clear enhancement in fire performance while keeping the mechanical properties within a range suitable for engineering use. The PA66 composites containing Eu@TA require a lower ADP loading to reach the V-0 classification, and the reduction in the PHRR and the increase in the FPI confirm the improvement in fire resistance. The change in combustion behavior is closely associated with the condensed-phase action of Eu@TA, which promotes earlier carbonization and stabilizes the char layer under high-temperature conditions. The residue formed during combustion becomes more compact and more graphitized, and phosphorus-containing fragments are incorporated into a crosslinked carbon network. Gas-phase analysis indicates that the presence of Eu@TA alters the release profile of volatile species, increasing the proportion of inert components and moderating the evolution of fuel-rich fragments. These features support the reduced combustion intensity observed in the calorimetry tests. The composite maintains tensile strength, elongation, and impact resistance at levels close to those of neat PA66, indicating that the introduction of Eu@TA does not cause pronounced embrittlement. The results demonstrate that a rare-earth–polyphenol coordination structure can function as an efficient partner to a phosphorus-based flame retardant, providing a practical path toward PA66 materials that combine improved flame retardancy with preserved mechanical performance. This bio-derived approach not only integrates sustainable polyphenolic sources with rare-earth catalysis for superior flame retardancy but also ensures long-term compatibility with biological macromolecules, offering a versatile framework for developing next-generation green polymers for high-safety industries.

Conflicts of interest

There are no conflicts to declare.

Data availability

The data supporting this article have been included as part of the supplementary information (SI). Supplementary information is available. See DOI: https://doi.org/10.1039/d6ra02012g.

Acknowledgements

This work was supported by the Natural Science Foundation Program of Xiamen (No. 3502Z202373074) and the STS Program of Chinese Academy of Sciences in Fujian Province (No. 2025T3005).

Notes and references

1 Y. Wang, L. Cui, J. Zhang, J. Shen, H. Xu, Z. Zhou, Y. Li and M. Zhu, *ACS Appl. Polym. Mater.*, 2025, **7**, 4677–4693.
2 B. Feng, S. Yu, H. Xiang, L. Li and M. Zhu, *Polymers*, 2025, **17**, 1074.
3 Y. Liu and Q. Wang, *Polym. Degrad. Stab.*, 2006, **91**, 3103–3109.
4 S. V. Levchik and E. D. Weil, *Polym. Int.*, 2000, **49**, 1033–1073.
5 C. Su, Y. Ren, P. Zhu, Y. Zhou, D. Wang and X. Dong, *Polym. Degrad. Stab.*, 2025, **240**, 111445.
6 Q. Hou, Y. Chen, J. Wang, M. Wu, H.-Y. Yu and X. Wang, *Int. J. Biol. Macromol.*, 2025, **307**, 142129.
7 J. Zeng, F. Lin, W. Hsu, S. Wang, Y. Wu, X. Wang, H. Cheng, Q. Zhu, H. Wu and L. Song, *Int. J. Biol. Macromol.*, 2024, **271**, 132636.
8 H. Cheng, Y. Wu, W. Hsu, F. Lin, S. Wang, J. Zeng, Q. Zhu and L. Song, *Int. J. Biol. Macromol.*, 2023, **253**, 127291.
9 Z. Zheng, J. L. Yao and Q. Yao, *Polym. Degrad. Stab.*, 2025, **240**, 111435.
10 A. R. Horrocks, G. Smart, S. Hörold, W. Wanzke, E. Schlosser and J. Williams, *Polym. Degrad. Stab.*, 2014, **104**, 95–103.
11 U. Braun, B. Schartel, M. A. Fichera and C. Jäger, *Polym. Degrad. Stab.*, 2007, **92**, 1528–1545.

12 Z. Zhan, M. Xu and B. Li, *Polym. Degrad. Stab.*, 2015, **117**, 66–74.
13 E. Gallo, B. Schartel, D. Acierno and P. Russo, *Eur. Polym. J.*, 2011, **47**, 1390–1401.
14 E. Gallo, U. Braun, B. Schartel, P. Russo and D. Acierno, *Polym. Degrad. Stab.*, 2009, **94**, 1245–1253.
15 A. D. Naik, G. Fontaine, F. Samyn, X. Delva, Y. Bourgeois and S. Bourbigot, *Polym. Degrad. Stab.*, 2013, **98**, 2653–2662.
16 S. Basak, A. S. M. Raja, S. Saxena and P. G. Patil, *Polym. Degrad. Stab.*, 2021, **189**, 109603.
17 X. Wang, G. Yang and H. Guo, *J. Anal. Appl. Pyrolysis*, 2023, **174**, 106111.
18 D. Écija, J. I. Urgel, A. P. Seitsonen, W. Auwärter and J. V. Barth, *Acc. Chem. Res.*, 2018, **51**, 365–375.
19 S. Mukherjee, K. M. A. Uddin, I. Turku, A. Rohumaa and J. Lipponen, *Resour. Environ. Sustain.*, 2025, **21**, 100229.
20 A.-N. Zhang, B.-W. Liu, H.-B. Zhao and Y.-Z. Wang, *Prog. Org. Coat.*, 2022, **170**, 106964.
21 Z. Tang, W. Chai, X. Su, Z. Zhang, M. Gao, Y. Li, Z. Han, X. Lv, J. He, H. Li and Z. Zheng, *J. Therm. Anal. Calorim.*, 2024, **149**, 9095–9107.
22 Z. Xia, A. Singh, W. Kiratitanavit, R. Mosurkal, J. Kumar and R. Nagarajan, *Thermochim. Acta*, 2015, **605**, 77–85.
23 L. Jiang, Y. Liu, C. Zuo, J. Zhao, W. Tan, Y. Ren and X. Liu, *Polym. Degrad. Stab.*, 2023, **217**, 110517.
24 X. Yu, L. He, X. Zhang, G. Bao, R. Zhang, X. Jin and D. Qin, *Int. J. Biol. Macromol.*, 2024, **265**, 130894.
25 P. Qi, R. Luo, T. Pichler, J. Zeng, Y. Wang, Y. Fan and K. Sui, *J. Hazard. Mater.*, 2019, **378**, 120721.
26 A.-N. Zhang, B.-W. Liu, H.-B. Zhao and Y.-Z. Wang, *ACS Appl. Mater. Interfaces*, 2022, **14**, 2345–2356.
27 Z. Tang, W. Chai, X. Su, Z. Zhang, M. Gao, Y. Li, Z. Han, X. Lv, J. He, H. Li and Z. Zheng, *RSC Adv.*, 2021, **11**, 14647–14663.
28 C. Feng, M. Liang, J. Jiang, Y. Zhang, J. Huang and H. Liu, *J. Anal. Appl. Pyrolysis*, 2016, **122**, 405–414.
29 A. Ramani and A. E. Dahoe, *Polym. Degrad. Stab.*, 2014, **105**, 1–11.
30 Y. Zhang, F. Lin, Y. Wu, S. Wang, Z. Liu and L. Song, *J. Appl. Polym. Sci.*, 2023, **140**, e53272.
31 A. Tewarson, *J. Fire Sci.*, 1994, **12**, 329–356.
32 M. Aaddouz, F. Laoutid, J. Mariage, B. Yada, A. Toncheva, J. Lazko, K. Azzaoui, R. Sabbahi, E. Mejdoubi, M. R. Saeb and P. Dubois, *ACS Sustainable Chem. Eng.*, 2025, **13**, 1450–1459.
33 Z. Zheng, J. L. Yao and Q. Yao, *Polym. Degrad. Stab.*, 2024, **228**, 110909.
34 Y. Li, B. Li, J. Dai, H. Jia and S. Gao, *Polym. Degrad. Stab.*, 2008, **93**, 9–16.
35 C. Wang, K. Gong, B. Yu and K. Zhou, *Compos. Part B: Eng.*, 2023, **265**, 110935.
36 B. Li, W. Hsu, T. Zheng, Y. Wu, S. Wang, F. Lin, L. Song and X. Rao, *Molecules*, 2025, **30**, 2102.
37 A. Deniz, N. Zaytoun, L. Hetjens and A. Pich, *ACS Appl. Polym. Mater.*, 2020, **2**, 5345–5351.
38 W. Xie, H. Chen, D. He, Y. Zhang, L. Fu, J. Ouyang and H. Yang, *Surf. Coat. Technol.*, 2019, **367**, 118–126.
39 X. Hu, X. Zhu and Z. Sun, *Constr. Build. Mater.*, 2020, **256**, 119445.
40 C.-H. Ke, J. Li, K.-Y. Fang, Q.-L. Zhu, J. Zhu, Q. Yan and Y.-Z. Wang, *Polym. Degrad. Stab.*, 2010, **95**, 763–770.
41 Y. Zhu, S. Cheng, W. Zhou, J. Jia, L. Yang, M. Yao, M. Wang, P. Wu, H. Luo and M. Liu, *ACS Appl. Mater. Interfaces*, 2017, **9**, 13173–13180.
42 H. Yang, B. Yu, P. Song, C. Maluk and H. Wang, *Compos. Part B: Eng.*, 2019, **176**, 107185.
43 S. Wang, Q. Fang, C. Liu, J. Zhang, Y. Jiang, Y. Huang, M. Yang, Z. Tan, Y. He, B. Ji, C. Qi and Y. Chen, *Eur. Polym. J.*, 2023, **187**, 111897.
44 D. Luo, Y. Liu, Y. Shi and Q. Wang, *J. Polym. Res.*, 2019, **26**, 216.
45 X. Ren, S. Long, X. Chen, X. Wang, X. Yang and H. Yu, *Int. J. Biol. Macromol.*, 2025, **289**, 138951.